CHEMISTRY OF MATERIALS

ARTICLE

pubs.acs.org/cm

Stability Study of a Magnesium β-Diketonate As Precursor for Chemical Vapor Deposition of MgO

Andrea Sartori,*[,†] Naida El Habra,[†,‡] Marco Bolzan,[†] Gilberto Rossetto,[†] Sergio Sitran,[†] Davide Barreca,[§] Alberto Gasparotto,[‡] and Maurizio Casarin[‡]

[†]ICIS—CNR, C.so Stati Uniti, 4-35127-Padova, Italy

[‡]Dipartimento di Scienze Chimiche, Università di Padova, Via Marzolo, 1-35131-Padova, Italy

[§]CNR-ISTM and INSTM, Dipartimento di Scienze Chimiche, Università di Padova, Via Marzolo, 1-35131-Padova, Italy

ABSTRACT: On the basis of the study of the thermal behavior of $[Mg(tmhd)_2(TMEDA)]$ (**1**; tmhd =2,2,6,6-tetramethyl-3,5-heptanedionate; TMEDA = *N*,*N*,*N*′,*N*′-tetramethylethylenediamine), a novel procedure for magnesium oxide thin film growth has been developed for chemical vapor deposition (CVD) applications. Complementary studies (thermogravimetric measurements and IR and NMR spectroscopy) enabled revelation of the dissociation of TMEDA from **1**, confirmed by the detection of both free TMEDA in the vapor phase and less volatile $[Mg_2(tmhd)_4]$ (**2**) as a residue after sublimation. The effect of this dissociation is an unwanted changeable sublimation rate of the precursor **1** during the CVD process. The endeavor of a constant deposition rate by simultaneously exploiting the good volatility of **1** was achieved through its synthesis *in situ* by using **2** with a diamine enriched carrier. Laser reflectance interferometry (LRI) measurements testified that such a method ensured a good and constant deposition rate throughout the growth experiment, independently of the adopted processing conditions. In addition, X-ray diffraction (XRD) measurements revealed the obtainment of textured and polycrystalline MgO coatings on sapphire and on Si(100). The system chemical composition was investigated by X-ray photoelectron spectroscopy (XPS).

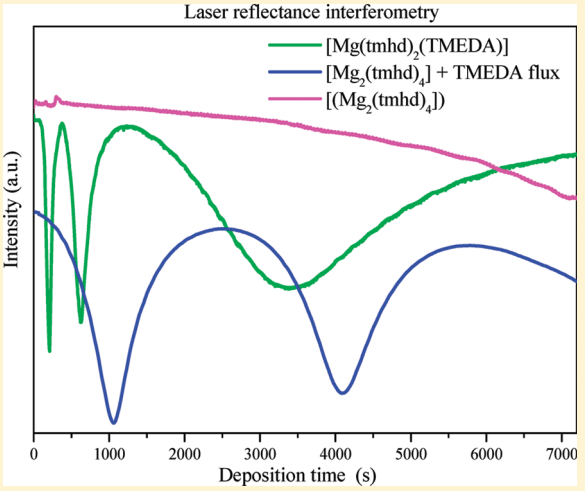

KEYWORDS: Chemical Vapor Deposition, Precursor Routes to Materials, Structural Characterization

INTRODUCTION

Magnesium oxide (MgO) thin films have attracted great scientific and technological interest in recent decades because of high MgO chemical and thermal stability (melting point = 2900 °C), a wide band gap (7.2 eV), and a low dielectric constant (9.8) and refractive index, as well as excellent thermal conductance and diffusion barrier properties.[1] This material has often been used for the production of protective coatings of dielectrics[2,3] and as buffer layers for superconducting or perovskite ferroelectric thin films.[4−9]

To date, MgO thin films have been deposited by several techniques, including sputtering,[10] laser ablation,[11−13] homogeneous precipitation,[14] sol−gel,[15,16] spray pyrolysis,[17−19] and chemical vapor deposition (atomic layer deposition (ALD),[20−23] plasma-enhanced chemical vapor deposition (PECVD),[24] pulsed organometallic molecular beam epitaxy (POMBE),[25] metal organic chemical vapor deposition (MOCVD)[26−41]). Among these techniques, MOCVD provides many advantages, including conformal coverage even on complex surface profiles, simplicity in experimental apparatuses and process control, good compositional tailoring, and suitability for a wide range of deposited materials.[41]

A key role in determining the success of the MOCVD thin film growth is played by the availability of highly volatile and thermally stable precursors, ensuring a constant and reproducible mass supply from the vapor phase to the substrate and a clean decomposition into the target material. Various organometallic and coordination compounds have been used as magnesium oxide CVD sources, including alkyls,[26−29] alkoxides,[30,31] carboxylates,[32] carbammates,[33,34] cyclopentadienyls,[35,36] and β-diketonates.[37−41] Among them, β-diketonates are very promising because of their stability, easy preparation, and clean decomposition pathway.[42] Nevertheless, when dealing with alkaline earth metals with a coordination number ≥ 6, the recurrent inability of β-diketonate ligands to saturate the metal coordination sphere may be compensated by oligomerization processes or by solvent coordination that, in turn, produce an unwanted increased melting point and a depressed volatility.

Received: July 26, 2010
Revised: October 7, 2010
Published: February 08, 2011

dx.doi.org/10.1021/cm1020788 | *Chem. Mater.* 2011, 23, 1113–1119

Such a problem may be tackled either by changing the precursor heating temperature or by making use of molecular engineering. With specific reference to the former possibility, it deserves to be emphasized that the use of high temperatures may be accompanied by decomposition of the complex and/or its sintering, thus leading to an instability of the precursor delivery rate during thin film depositions. Concerning chemical modifications, two different strategies can be adopted to increase the β-diketonate compounds' volatility: (i) inhibiting intermolecular interactions by modifying the ligand skeleton through the introduction of a sterically hindered moiety (e.g., tmhd vs acetylacetonate) or by using fluorinated ligands such as hfa (hfa = 1,1,1,5,5,5-hexafluoro-2,4-pentanedionate); (ii) employing chelating ligands able to saturate the metal ion coordination sphere.[1,21,42] Despite the presence in the literature of several modified magnesium β-diketonates ($[Mg_2(tmhd)_4]$, $[Mg(tmhd)_2(TMEDA)]$, and $[Mg(hfa)_2(TMEDA)]$)[1,37,43] employed as MOCVD volatile precursors, the majority of studies referred to the less volatile dimeric compound **2**. In this paper, the attention has been focused on **1** and **2**, whereas the use of the fluorinated β-diketonate was discarded to prevent possible fluorine incorporation in the target material.[44,45] In particular, a method for the CVD of MgO, based on the study of the thermal behavior of these two complexes, is proposed.

Precursor **1**, designed and used for the first time by the Marks' group,[43] is easily obtainable from **2** and it has been claimed that it possesses superior thermal properties for use in CVD applications thanks to its monomeric structure, enabled by the complete saturation of the Mg(II) coordination sphere.[43,46] Before going on, it is noteworthy that the outcomes of our thermogravimetric, NMR, and IR measurements on complex **1** ultimately testify to its instability, which determines a nonconstant precursor evaporation rate, resulting, in turn, in a difficult and nonreproducible process control. In other words, even though we are perfectly aware that **1** can be successfully used as a CVD precursor,[43] the effect of the above-mentioned instability might cause a nonconstant precursor evaporation rate. In order to afford a constant MgO deposition rate, in the present study, we propose the *in situ* synthesis of the volatile complex **1** by adopting **2** as a precursor and working with a large TMEDA excess in the carrier gas flow to prevent the possible dissociation of **1**. To the best of our knowledge, such a method has never been reported in the literature in the case of the target Mg complexes. As shown in this manuscript, the adopted approach results in a constant and reproducible film growth rate of 4 nm/min.

EXPERIMENTAL SECTION

General Methods. Htmhd (Fluka) and the other starting materials for the synthesis of precursors (Aldrich) were used as received. To avoid the possible decomposition of **2** and **1**, all manipulations after drying and sublimation of the products were made under dry conditions using a nitrogen-filled drybox. ^{1}H NMR spectra were recorded by using a Bruker AMX 300 (300 MHz) spectrometer, and proton spectra were referred to the protio impurities of the deuterated solvent (the obtained chemical shifts were computed with respect to TMS). Thermogravimetric measurements were carried out in a nitrogen atmosphere by using Netzsch STA 449 thermoanalytical equipment (flow rate = 50 mL $\times$ min^{-1}; heating rate = 1.50 °C $\times$ min^{-1}; sample weight $\approx$ 30 mg. Isothermal mass loss determination (195 °C) was carried out for 8 h in a nitrogen atmosphere using heating rates of 10 and 1 °C $\times$ min^{-1} in the temperature ranges 20−185 and 185−195 °C, respectively.

FT-IR spectra were recorded on an ATI Mattson, Genesis spectrometer operating in transmittance mode at normal incidence (resolution = 2 cm^{-1}). Room temperature spectra were collected on KBr pellets, while vapor phase spectra were collected in the 100−225 °C range using a heated gas cell Storm 10H (Specac) with NaCl windows (path length = 10 cm, volume = 114 cm^3). The temperature was measured by means of a K-type thermocouple introduced into the cell. Prior to each measurement, a glass boat with ~30 mg of the precursor was introduced into the cell, which was filled with argon at ambient pressure. In each spectrum, the background contribution was subtracted.

Synthesis of $[Mg_2(tmhd)_4]$ (2). The characteristics of **2** have been reported to be dependent on synthesis methods and storage conditions.[21] In this work, synthesis, purification, and characterization of **2** have been carried out by adopting a procedure similar to that of Hatanpää et al.[21,47] In more detail, $Mg(NO_3)_2 \cdot 6H_2O$ (2.56 g, 10 mmol) was dissolved in 10 mL of deionized water. Subsequently, a suspension prepared by adding Htmhd (4.12 mL, 20 mmol) to 30 mL of a NaOH solution (0.8 g, 20 mmol) in ethanol/water (volume ratio = 1:2) was added. The formed white precipitate was filtered, washed several times with water, and dried under reduced pressure. The product was purified by sublimation under vacuum conditions at 100 °C/10^{-2} mbar and characterized by ^{1}H NMR [^{1}H NMR (C_6D_6), δ (ppm): 5.88 (2H, s, CH), 1.24 (36H, bs, CH_3)].

Synthesis of $[Mg(tmhd)_2(TMEDA)]$ (1). Analogously to **2**, the synthesis, purification, and characterization of **1** have been carried out by adopting a similar procedure to the procedures reported by Babcock et al.[43,48] More specifically, TMEDA (1.0 equiv) was added to a $Mg(NO_3)_2 \cdot 6H_2O$ solution in 10 mL of deionized water. The preparation of the Htmhd suspension and the successive product purification (without sublimation step) were carried out as described for **2**. The product was characterized by comparison of its ^{1}H NMR spectrum with literature data.[43] [^{1}H NMR (C_6D_6), δ (ppm): 5.75 (2H, s, CH), 2.20 − 2.10 (16H, bd, TMEDA), 1.28 (36H, s, CH_3)].

MgO Thin Film Growth. MgO thin films were grown in a cold-wall low pressure MOCVD reactor. The vapors of precursor **2** were transported into the reaction chamber through an especially designed effusion cell maintained at 195 °C. Prior to entering the cell, N_2 carrier gas (2 sccm) was fluxed through a TMEDA-containing bubbler kept at 35 °C. Coreagent gas, a blend of O_2 (30 sccm) and $N_2 + H_2O$ vapors (2 sccm of N_2 bubbled through a water reservoir kept at 30 °C), was mixed with the precursor flow immediately upstream of the susceptor (distance = 3 cm).[49] Different substrate temperatures (550 and 670 °C) were investigated using a 1" ceramic heater under a total working pressure of 10 mbar. For comparison, growth processes were also carried out starting from precursor **1**. In this case, the carrier gas was not fluxed through the TMEDA bubbler.

Before each deposition, the Si(100) substrates (SI-MAT) were rinsed in acetone and deionized water, whereas sapphire substrates (MaTeck) were used as purchased.

After deposition, the samples were stored under nitrogen to limit possible film carbonatation. The reproducibility of the obtained results was checked by repeating several deposition experiments under the same conditions.

Film Characterization. Film thickness was determined by profilometer analysis and laser reflection interferometry (LRI). The former was carried out by employing a KLA-Tencor Alpha-Step IQ surface profiler to analyze the film height steps on partially masked samples after the deposition, while the latter allowed a noninvasive *in situ* monitoring of film growth by analyzing the number of fringes characterizing the interferogram and by applying the following approximate equation:

$$d = \frac{m\lambda}{2n_1 \cos \theta_r} \quad (1)$$

where d, m, λ, n_1, and θ_r correspond to the film thickness, the fringe order, the laser wavelength (635 nm), the film refractive index, and the refracted angle, respectively.[50]

LRI measurements were recorded only on Si(100) (n = 3.4), because the similar refraction index values of MgO (n = 1.74) and sapphire (n = 1.76) prevent the observation of interference fringes.[51]

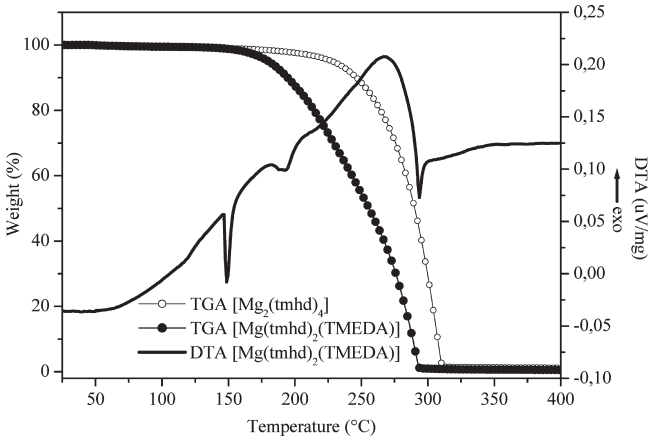

Figure 1. Comparison of thermal behaviors of $[Mg(tmhd)_2(TMEDA)]$ (**1**) and $[Mg_2(tmhd)_4]$ (**2**) recorded by TGA measurements.

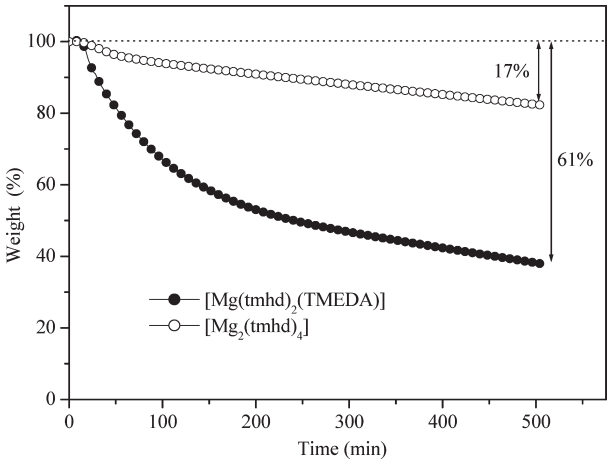

Figure 2. Isothermal data collected at 195 °C of $[Mg(tmhd)_2(TMEDA)]$ (**1**) and $[Mg_2(tmhd)_4]$ (**2**). The corresponding weight losses (%) at the end of the measurement (after 500 min) are reported.

X-ray diffraction (XRD) measurements were performed using a Philips PW3020 powder diffractometer in Bragg−Brentano $\theta-2\theta$ geometry, using Cu Kα radiation (40 kV, 30 mA, λ = 1.54056 Å). The patterns were collected in the 15−85° 2θ range. Peak positions were determined with a statistical uncertainty of 0.02°. Phase identification was obtained with the support of standard ICDD files.

X-ray photoelectron spectroscopy (XPS) spectra were recorded on a Perkin-Elmer Φ 5600ci spectrometer at a pressure lower than 10^{-9} mbar using nonmonochromatized Al Kα (1486.6 eV) and Mg Kα (1253.6 eV) excitation sources. In particular, since in the case of the Al Kα source the nitrogen N 1s signal [Binding Energy (BE) ≈ 400 eV) is overlapped with the Mg KLL one, the Mg Kα source was used to unambiguously evaluate the presence/absence of this element. The spectrometer was calibrated by assigning to the Au $4f_{7/2}$ line a BE of 84.0 eV with respect to the Fermi level. The estimated standard deviation for BEs was ±0.2 eV. The atomic compositions were evaluated by using sensitivity factors provided by the Φ V5.4A software. In order to obtain a more accurate evaluation of atomic percentages, the Mg 2p signal was used in the quantification instead of the more intense Mg 1s photopeak, due to its appreciable BE difference with respect to the O and C peaks. This feature would imply the analysis of photoelectrons with different escape depths, yielding thus an uncorrected estimation.[52] Ar^+ sputtering was carried out at 3.5 kV and a 0.5 mA × cm^{-2} beam current density, with an argon partial pressure of 4 × 10^{-8} mbar. Before analysis, samples were stored under nitrogen and directly introduced into the analysis chamber using a fast entry lock system.

RESULTS AND DISCUSSION

In order to preliminarily analyze the behavior of **1** and **2**, a series of thermogravimetric measurements has been carried out. An inspection of Figure 1, where the thermogravimetric analyses (TGA) of **1** and **2** are reported, clearly shows that **1** remains almost stable up to 160 °C, while it undergoes a remarkable weight loss (99%) above this temperature. Despite the absence of two clearly defined steps in the TGA of **1**, a careful inspection of the experimental curve allows the identification of two different curve slopes. In this regard, it is noteworthy that the differential thermal analysis (DTA) curve of **1** (see Figure 1), besides the two endothermic maxima corresponding to its melting (150 °C) and sublimation (294 °C) temperatures, includes a further broad peak at ∼193 °C, which could be representative of a possible dissociative process of **1**.

Figure 2 shows the isothermal analysis pertaining to **1** and **2** collected at 195 °C. As regards compound **2**, a sublimation with a 17% weight loss after 500 min was observed. For compound **1**, the recorded weight loss corresponds to 31, 46, and 61% after 100, 200, and 500 min, respectively. In addition, the curve slope becomes almost constant after 250 min, and subsequently, the sublimation process is slower up to the end of the experiment. The rationale for such behavior has been obtained through the analysis of residual products. As a matter of fact, the peaks that originated in the ^{1}H NMR spectrum of **1** with tmhd methyl (Figure 3a) and methine (Figure 3b) protons are shifted to lower and higher fields, respectively, when compared to the corresponding signals of **2**. Interestingly, the ^{1}H NMR spectrum of the complex **1** sublimation residue (collected at 100 °C/10^{-2} mbar) reveals the presence of two different groups of signals, possibly due to the contemporary presence of **1** and **2**. On the other hand, the spectrum of the residue remaining after isothermal measurements at 195 °C/1013 mbar shows the complete disappearance of TMEDA peaks (2.20−2.10 ppm). In this case, the chemical shift related to the tmhd methyl and methine protons is not the same as that of the starting compound, since these peaks are perfectly overlapped with the signals of **2**.

Taken together, the outcomes of NMR and thermal analyses suggest that **1** undergoes a partial dissociation during the sublimation, involving the TMEDA ligand detachment (DTA broad peak at 193 °C, see Figure 1). Nevertheless, such a process cannot be the sole responsibility of the observed weight loss related to the isothermal curve of **1** (61% in Figure 2), because for a complete TMEDA dissociation, the mass reduction should amount to a 23% (PM_{TMEDA}: 116.208 g/mol; PM_1: 507.037 g/mol). On the other hand, the remaining 61 − 23 = 38% cannot be ascribed only to the volatilization of **2** (formed upon TMEDA detachment), because in this case the maximum weight loss would have been less than 17% (Figure 2). Indeed, an additional weight loss occurs, which cannot be ascribed to the sole contribution of TMEDA and $[Mg_2(tmhd)_4]$. As a matter of fact, it is reasonable to hypothesize that even a low amount of $[Mg(tmhd)_2(TMEDA)]$ sublimes without decomposition, thus explaining the observed behavior. After 200−250 min, the slopes of the isothermal curves of **1** and **2** are very similar, thus suggesting that TMEDA is completely removed and the weight loss is only due to the sublimation of the less volatile **2**.

All of the reported NMR spectra show the loss of TMEDA in **1** residue. In a different way, NMR analyses of the sublimation

dx.doi.org/10.1021/cm1020788 |*Chem. Mater.* 2011, 23, 1113–1119

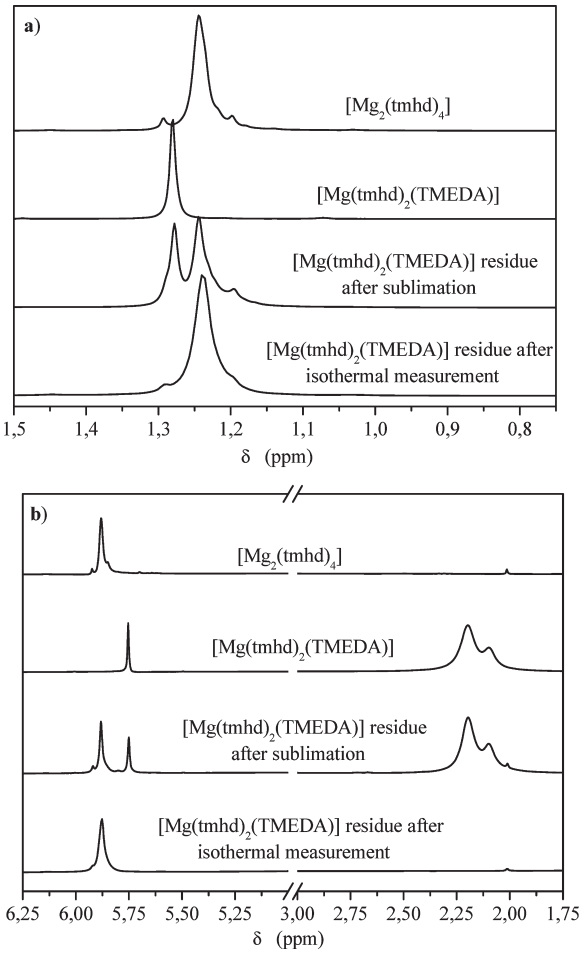

Figure 3. ^{1}H NMR spectra of $[Mg(tmhd)_2(TMEDA)]$ (**1**) and $[Mg_2(tmhd)_4]$ (**2**) related to the region of (a) methyl and (b) methine and TMEDA signals, as a function of the treatment conditions.

product of precursor **1**, collected from a coldfinger surface at 100 °C/10^{-2} mbar,[53] revealed the presence of the only diamine adduct without evidence of free TMEDA or **2** (incidentally, this behavior was observed even by Hatampää et al.[46]). A possible explanation for this apparent contradiction (*i.e.*, the evidence of only **1** in the coldfinger as well as the evidence of **1**'s decomposition in the residue) is that only a negligible amount of **2** sublimes and free TMEDA does not condense on the coldfinger surface, so that only **1**'s signals are observed.

The presence of the free TMEDA among the sublimation products of **1** has been ascertained using IR spectroscopy (see Figure 4). In particular, a series of IR spectra have been recorded at different temperatures. In the range 3800−700 cm^{-1}, the spectra of TMEDA and complex **2** do not undergo significant variations when recorded at room temperature or in the vapor phase. More specifically, the comparison of the FT-IR spectra of **1** in KBr pellets at 25 °C and in the vapor phase at 200 °C with those of **2** and of TMEDA allowed us to discriminate between **1** and **2** (note the absence in **2** of the TMEDA C−H stretching absorption —ν_{CH}—at 2792 cm^{-1}). In this regard, it can be useful to point out that, in the recent past, some of us[54] ascribed the quite low frequency of this stretching to charge donation effects from the nitrogen lone pair (n) to the antibonding σ^* orbital of the *trans* C−H bond ($n-\sigma^*$ interaction). The blue shift (Δ = 14 cm^{-1}) undergone by ν_{CH} upon coordination can be explained by

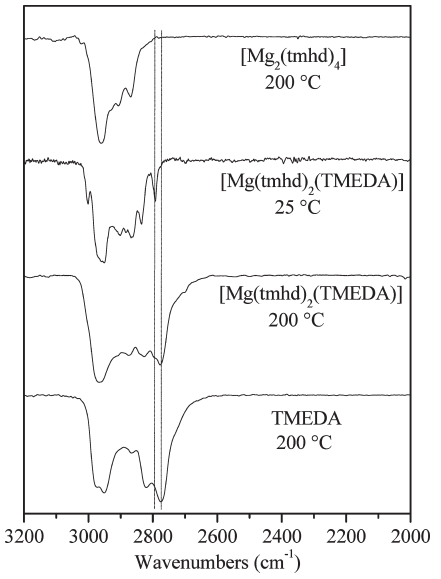

Figure 4. Comparison of FT-IR spectra of $[Mg(tmhd)_2(TMEDA)]$ (**1**), $[Mg_2(tmhd)_4]$ (**2**), and TMEDA in the range 2000−3200 cm^{-1}.

referring to the N → Mg donation which strengthens the *trans* C−H bond on passing from the free ligand to the coordinated one. Finally, the comparison between the vapor phase (at 200 °C) and room temperature FT-IR spectrum of **1** confirms its partial dissociation. In fact, the copresence of the absorptions at 2778 and 2792 cm^{-1} ultimately testifies to the coexistence of both **1** and TMEDA.[55] Furthermore, despite the isothermal measurements (see Figure 2) being consistent with the sublimation of **2** (weight loss = 17%), the lack of any FT-IR characteristic intense peaks prevents the unambiguous identification of **2** in the vapor phase.

All of the outcomes so far discussed clearly indicate the dissociation of TMEDA from **1** at relatively mild sublimation temperatures (NMR 100 °C/10^{-2} mbar, vapor phase IR 100 °C/1013 mbar): for this reason, this complex could not be a suitable Mg source to guarantee an accurate control of the MgO deposition process and a reproducible growth rate. This is further confirmed, under the adopted growth conditions, by the LRI[56] results pertinent to a film grown by using **1** as a precursor (Figure 5). More specifically, the increasing spacing between one fringe and another is in tune with a decreasing growth rate during the deposition process. In particular, the initial fast film growth followed by a significant deposition rate reduction could be the result of the gradual decomposition of **1** into the less volatile **2**. Incidentally, different precursor temperatures (from 175 to 220 °C in order to obtain a reasonable growth rate) generate very similar LRI curves.

On this basis, an alternative method to improve the MgO deposition could be that of employing **2** as precursor and a reactive gas carrier generated by fluxing N_2 into a bubbler containing liquid TMEDA. The use of a reactive gas was already reported by Buriak et al.[57] and by Zhang et al.,[58] which introduced an ammonia flow to improve the volatility of barium ($[Ba_4(tmhd)_8]$ and $[Ba(acac)_2]_n$, with acac = acetylacetonate) and calcium ($[Ca_3(tmhd)_6]$) complexes, respectively. In the present work, the continuous TMEDA ligand supply results in an *in situ* reaction with **2**, producing the more volatile **1**. At variance with the above-discussed case, such an approach produced an almost regular spacing among the LRI fringes (Figure 5), thus indicating that the introduction of TMEDA as a

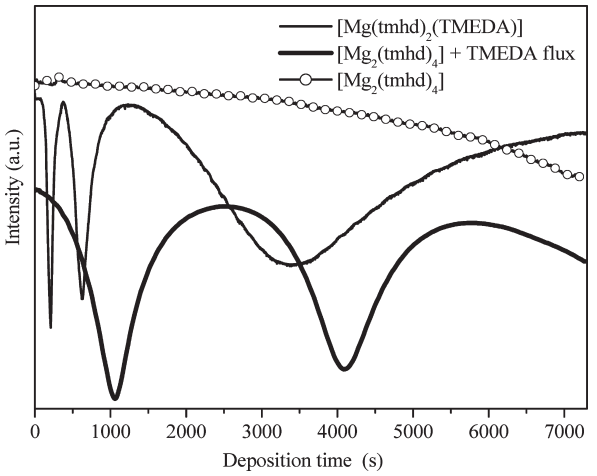

Figure 5. Typical *in situ* LRI traces recorded at 195 °C during the CVD of MgO from $[Mg(tmhd)_2(TMEDA)]$ (**1**), from $[Mg_2(tmhd)_4]$ (**2**), and from a TMEDA reactive gas fluxed on $[Mg_2(tmhd)_4]$.

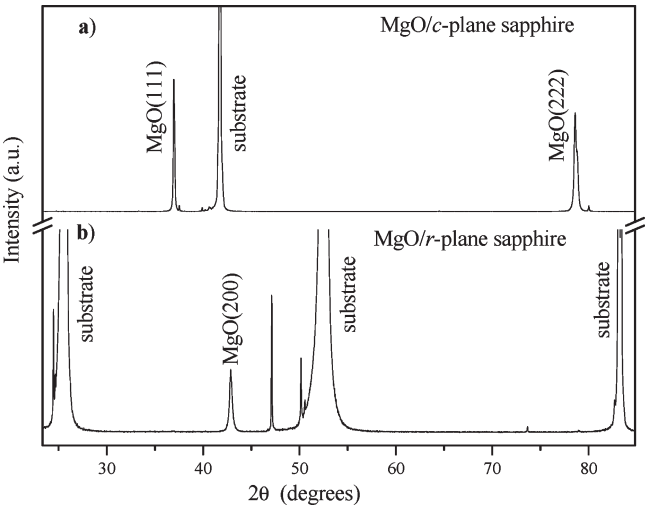

Figure 6. X-ray diffraction of the MOCVD MgO film with the use of a TMEDA reactive gas fluxed on $[Mg_2(tmhd)_4]$ (**2**) on (a) *c*-plane sapphire and (b) *r*-plane sapphire.

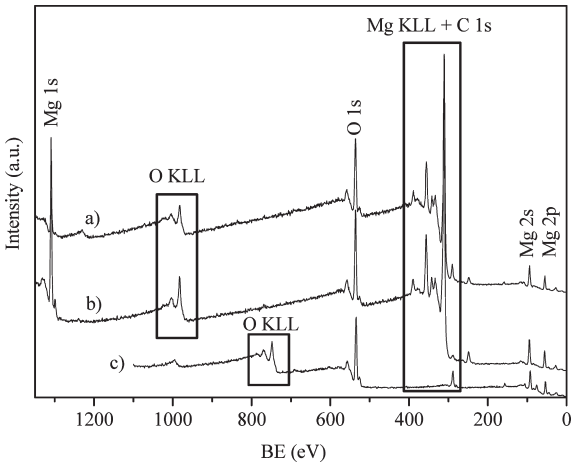

Figure 7. XPS survey spectra of an MgO film deposited on *c*-plane sapphire at 550 °C: (a) surface (Al Kα source), (b) after 10′ Ar^+ erosion (Al Kα source), (c) surface (Mg Kα source).

reactive gas is an effective means to maintaining a constant deposition rate as well as to improving the deposition process control. The excess of the unreacted TMEDA is eliminated with the gas flow avoiding any film contamination, as testified to by the XPS analysis (see below). In a different way, the use of **2** without TMEDA (Figure 5) does not result in easily detectable fringes during the process, but only in a slight and progressive intensity decrease. Such a behavior suggests a limited film thickness, *i.e.* a modest growth rate, under these conditions. It can be concluded that the combined use of **2** and TMEDA vapors increases the precursor volatility, yielding a reproducible growth rate of ∼4 nm/min.

The film microstructure was investigated using XRD measurements. The corresponding pattern of the as-grown MgO thin films on *c*-plane sapphire (Figure 6a) is characterized by the presence of two dominant peaks at $2\theta = 36.93°$ and 78.66° assignable to the (111) and the (222) planes of a *periclase* cubic-type MgO crystal (ICDD pattern No. 01-077-2179). This evidence is indicative of a predominant (111) preferential orientation at both 550 and 670 °C growth temperatures. Alternatively, MgO thin film growth on *r*-plane sapphire (Figure 6b) shows only one peak at $2\theta = 42.88°$ related to the (200) cubic-type MgO reflection, indicating a strong (200) preferential orientation.

At variance with the deposition on sapphire, films deposited on Si(100) are poorly crystalline and do not display any dominant orientation. XRD reflections lying at $2\theta = 36.93°$, 42.88°, 62.30°, and 78.66° are ascribed to (111), (200), (220), and (222) planes of the MgO cubic structure. No significant variations in the relative XRD peak intensity were observed at different deposition temperatures (550 and 670 °C).

Purity and chemical compositions of the obtained films have been assessed by means of XPS measurements. As an example, Figure 7 reports representative data for a film supported on *c*-plane sapphire. No appreciable N 1s peaks could ever be observed, whereas Mg, C, and O signals were detected both on the surface (at. % 31, 24, and 45, respectively) and after Ar^+ erosion (at. % 39, 8, 53, respectively). It is worth noticing that, upon erosion, the C content underwent a significant reduction. The remaining carbon percentage (8%) could arise from a partial implantation of surface C contaminants induced by Ar^+ ions in the inner sample layers, suggesting thus that the contribution to the contamination was the sample manipulation prior to XPS analyses.

In regards to surface spectra, the C 1s signal was characterized by a main band centered at 284.8 eV arising from adventitious carbon,[59,60] whereas a further weak contribution at 288.5 eV was related to the formation of magnesium carbonate.[36,61,62] The O 1s surface peak displayed an asymmetric shape, with a tailing on its higher BE side. According to the literature, the main component centered at 530.1 eV was ascribed to lattice oxygen in MgO, while the latter minor contribution in the 531.3−531.6 eV energy interval was traced back to the presence of hydroxyl species, arising from air exposure and related to the high MgO affinity toward moisture. Such an assignment is in agreement with an O/Mg ratio (≈1.4) appreciably higher than the stoichiometric value expected for pure MgO. The contribution of magnesium carbonates to the O 1s photopeak (expected position 532.2−533.5 eV) was very low, as also suggested by the C 1s peak analysis.[36,61−66] The shape and position of the Mg 2p (BE = 49.8 eV) and Mg 1s (BE = 1302.7−1302.9 eV) signals were in agreement with the presence of MgO as the main phase.[36,61−63,66,67]

dx.doi.org/10.1021/cm1020788 |*Chem. Mater.* 2011, 23, 1113–1119

Most of the previous considerations regarding the film surface composition still hold after 10 min of Ar^+ sputtering. In fact, the main differences upon erosion are limited to (i) an appreciable reduction of the carbon atomic percentage, suggesting that the synthesized films are of good purity; (ii) a significant O/Mg ratio reduction (≈1.1), due to both preferential sputtering[52] and the removal of surface hydroxyl groups. Finally, it is important to underline that no nitrogen signals have ever been detected, as better evidenced by the survey spectra collected with a Mg Kα source (N 1s peak expected at ∼400 eV). Overall, these observations highlight a high purity of the obtained MgO films.

CONCLUSIONS

In this work, the behavior of the complex $[Mg(tmhd)_2(TMEDA)]$ as a potential CVD precursor of MgO films was studied using several techniques. The obtained results evidenced the thermodynamic instability of **1**, which generates TMEDA and $[Mg_2(tmhd)_4]$ and determines an irreproducible mass supply and an uncontrolled film deposition rate. Such a problem has been overcome through a novel, alternative procedure exploiting **2** as precursor and TMEDA fluxed by N_2 as a reactive gas carrier, which allows a constant evaporation rate throughout the growth duration thanks to the *in situ* generation of **1**. XRD patterns of the obtained deposits show the formation of a textured MgO *periclase* cubic structure on sapphire and silicon substrates. The films did not display significant incorporation of carbon and nitrogen in the MgO phase.

AUTHOR INFORMATION

Corresponding Author

*Author to whom correspondence should be addressed. E-mail: Andrea.Sartori@icis.cnr.it.

ACKNOWLEDGMENT

The skillful cooperation of Mr. Valerio Corrado is gratefully acknowledged. FISR−MIUR Project "Inorganic and hybrid nanosystems for the development and innovation of fuel cells" is gratefully acknowledged for financial assistance.

REFERENCES

(1) Wang, L.; Yang, Y.; Ni, J.; Stern, C. L.; Marks, T. J. *Chem. Mater.* **2005**, *17*, 5697.
(2) Renault, O. Ph.D. Thesis; Institut National Polytechnique de Grenoble, Grenoble, France, 1998.
(3) Andoh, S.; Murase, K.; Umeda, S.; Nakayama, N. *IEEE Trans. Electron Devices* **1976**, *23*, 319.
(4) Hinds, B. J.; McNeely, R. J.; Chen, J.; Dias, C.; Studebaker, D. L.; Marks, T. J.; Hogan, T. P.; Schindler, J. L.; Kannewurf, C. R. *J. Alloys Compd.* **1997**, *251*, 328.
(5) Musolf, J.; Boeke, E.; Waffenschmidt, E.; He, X.; Heuken, M.; Heime, K. *J. Alloys Compd.* **1993**, *195*, 295.
(6) Tonouchi, M.; Sakaguchi, Y.; Kobayashi, T. *J. Appl. Phys.* **1987**, *62*, 961.
(7) Nashimoto, K.; Fork, D. K.; Geballe, T. H. *Appl. Phys. Lett.* **1992**, *60*, 1199.
(8) Basit, N. A.; Kim, H. K.; Blachere, J. *Appl. Phys. Lett.* **1998**, *73*, 3941.
(9) Yoon, J.-G.; Kim, K. *Appl. Phys. Lett.* **1996**, *68*, 2523.
(10) Lee, J. H.; Eun, J. H.; Park, S. Y.; Kim, S. G.; Kim, H. J. *Thin Solid Films* **2003**, *435*, 95.
(11) Stampe, P. A.; Kennedy, R. J. *J. Cryst. Growth* **1998**, *191*, 472.
(12) Stampe, P. A.; Kennedy, R. J. *J. Cryst. Growth* **1998**, *191*, 478.
(13) Stampe, P. A.; Kennedy, R. J. *Thin Solid Films* **1998**, *326*, 63.
(14) Park, J. S.; Han, Y. H. *J. Eur. Ceramic. Soc.* **2007**, *27*, 1077.
(15) Rywak, A. A.; Burlitch, J. M. *Chem. Mater.* **1995**, *7*, 2028.
(16) Menon, M.; Bullard, J. W. *J. Mater. Chem.* **1999**, *9*, 949.
(17) Stryckmans, O.; Segato, T.; Duvigneaud, P. H. *Thin Solid Films* **1996**, *283*, 17.
(18) Fu, X.; Wu, G.; Song, S.; Song, Z.; Duo, X.; Lin, C. *Appl. Surf. Sci.* **1999**, *148*, 223.
(19) Kim, S. G.; Kim, J. Y.; Kim, H. J. *Thin Solid Films* **2000**, *376*, 110.
(20) Putkonen, M.; Johansson, L.-S.; Rauhala, E.; Niinisto, L. *J. Mater. Chem.* **1999**, *9*, 2449.
(21) Hatampää, T.; Ihanus, J.; Kansikas, J.; Mutikainen, I.; Ritala, M.; Leskela, M. *Chem. Mater.* **1999**, *11*, 1846.
(22) Putkonen, M.; Sajavaara, T.; Niinisto, L. *J. Mater. Chem.* **2000**, *10*, 1857.
(23) Burton, B. B.; Goldstein, D. N.; George, S. M. *J. Phys. Chem. C* **2009**, *113*, 1939.
(24) Fujii, E.; Tomozawa, A.; Torii, H.; Takayama, R.; Nagaki, M.; Narusawa, T. *Thin Solid Films* **1999**, *352*, 85.
(25) Dean, K. A.; Buchholz, D. B.; Marks, L. D.; Chang, R. P. H.; Vuchic, B. V.; Merkle, K. L.; Studebaker, D. B.; Marks, T. J. *J. Mater. Res.* **1995**, *10*, 2700.
(26) Huang, R.; Kitai, A. H. *Appl. Phys. Lett.* **1992**, *61*, 1450.
(27) Sung, M. M.; Kim, C.; Kim, C. G.; Kim, Y. *J. Cryst. Growth* **2000**, *210*, 651.
(28) Lee, S. S.; Lee, S. Y.; Hyun, J. S.; Kim, C. G.; Kim, Y. *Chem. Vap. Deposition* **2002**, *8*, 257.
(29) Lee, S. Y.; Lee, S. H.; Nah, E. J.; Lee, S. S.; Kim, Y. *J. Cryst. Growth* **2002**, *236*, 635.
(30) Maruyama, T.; Shionoya, J. *Jpn. J. Appl. Phys.* **1990**, *29*, L810.
(31) Davies, H. O.; Jones, A. C.; Leedham, T. J.; Crosbie, M. J.; Wright, P. J.; Boag, N. M.; Thompson, J. R. *Chem. Vap. Deposition* **2000**, *6*, 71.
(32) Vallet-Regí, M.; Labeau, M.; García, E.; Cabañas, M. V.; González-Calbet, J. M.; Delabouglise, G. *Physica C* **1991**, *180*, 57.
(33) Hill, M. R.; Jones, A. W.; Russel, J. R.; Roberts, N. K.; Lamb, R. N. *J. Mater. Chem.* **2004**, *14*, 3198.
(34) Hill, M. R.; Lee, E. Y. M.; Russel, J. R.; Wang, Y.; Lamb, R. N. *J. Phys. Chem.* **2006**, *110*, 9236.
(35) Musolf, J.; Boeke, E.; Waffenschmidt, E.; He, X.; Heuken, M.; Heime, K. *J. Alloys Compd.* **1993**, *195*, 295.
(36) Carta, G.; El Habra, N.; Crociani, L.; Rossetto, G.; Zanella, P.; Zanella, A.; Paolucci, G.; Barreca, D.; Tondello, E. *Chem. Vap. Deposition* **2007**, *13*, 185.
(37) Lu, Z.; Feigelson, R. S.; Route, R. K.; DiCarolis, S. A.; Hiskes, R.; Jacowitz, R. D. *J. Cryst. Growth* **1993**, *128*, 788.
(38) Boo, J.-H.; Yu, K.-S.; Koh, W.; Kim, Y. *Mater. Lett.* **1996**, *26*, 233.
(39) Boo, J.-H.; Lee, S.-B.; Yu, K.-S; Koh, W.; Kim, Y. *Thin Solid Films* **1999**, *341*, 63.
(40) Zeng, J. M.; Wang, H.; Shang, S. X.; Wang, Z.; Wang, M. *J. Cryst. Growth* **1996**, *169*, 474.
(41) Cheng, J.; Meng, X.; Yang, P.; Chu, J. *J. Cryst. Growth* **1998**, *194*, 89.
(42) Jones, A. C. *J. Mater. Chem.* **2002**, *12*, 2576.
(43) Babcock, J. R.; Benson, D. D.; Wang, A.; Edleman, N. L.; Belot, J. A.; Metz, M. V.; Marks, T. J. *Chem. Vap. Deposition* **2000**, *6*, 180.
(44) Zhang, J. M.; Wessels, B. W.; Richeson, D. S.; Marks, T. J.; DeGroot, D. C.; Kannewurf, C. R. *J. Appl. Phys.* **1991**, *69*, 2743.
(45) Malandrino, G.; Richeson, D. S.; Marks, T. J.; DeGroot, D. C.; Schindler, J. L.; Kannewurf, C. R. *Appl. Phys. Lett.* **1991**, *58*, 182.
(46) Hatanpää, T.; Kansikas, J.; Mutikainen, I.; Leskelä, M. *Inorg. Chem.* **2001**, *40*, 788.
(47) More specifically, Hatampää et al. reported the reaction of an aqueous ethanolic solution of $MgSO_4$ with Na(tmhd).
(48) More specifically, Babcock et al. used $MgSO_4$ as a basic reagent.
(49) The position and the temperature at which the carrier gas was mixed with the coreagent gas should prevent the possible formation of precursor $Mg(tmhd)_2 \cdot 2(H_2O)$, investigated by: Maria, M.; Selvakumar, J.; Raghunathan, V. S.; Nagaraja, K. S. *Surf. Coat. Technol.* **2009**, *204*, 222.

(50) Ohring, M. *Materials Science of Thin Fims*, 2nd ed.; Academic Press: London, 2002; p 567.
(51) Lide, D. R. *Handbook of Chemistry and Physics*, 72nd ed.; CRC Press: Boca Raton, FL, 1991.
(52) Briggs, D.; Seah, M. P. *Practical Surface Analysis*, 2nd ed.; J. Wiley & Sons: New York, 1990.
(53) The presence of $[Mg(tmhd)_2(TMEDA)]$ as sublimation product collected from a coldfinger surface was observed even at 200 °C at room pressure using ^1H NMR measurements.
(54) Bandoli, G.; Barreca, D.; Gasparotto, A.; Seraglia, R.; Tondello, E.; Devi, A.; Fischer, R. A.; Winter, M.; Fois, E.; Gamba, A.; Tabacchi, G. *Phys. Chem. Chem. Phys.* **2009**, *11*, 5998.
(55) The dissociation for complex **1** was observed throughout the investigated temperature range (100−225 °C).
(56) The LRI technique is based on the reflection of monochromatic radiation incident on the sample during the growth. The detected beam intensity results from the interference of rays reflected from different interfaces (air/film and film/substrate). Fringes are the result of subsequent constructive and destructive interferences, and their formation mainly depends on the different optical paths of the two beams, as well as on the material growth rate. Moreover, the distance between maxima of successive fringes allows a qualitative evaluation of the deposition rate constancy.
(57) Buriak, J. M.; Cheatham, L. K.; Graham, J. J.; Gordon, R. G.; Barron, A. R. *Mater. Res. Soc. Symp. Proc.* **1991**, *204*, 545.
(58) Zhang, J. M.; DiMeo, F.; Wessels, B. W.; Schulz, D. L.; Marks, T. J.; Schindler, J. L.; Kannewurf, C. R. *J. Appl. Phys.* **1992**, *71*, 2769.
(59) Moulder, J. F.; Stickle, W. F.; Sobol, P. E.; Bomben, K. D. *Handbook of X-Ray Photoelectron Spectroscopy*; Perkin Elmer Corporation: Eden Prairie, MN, 1992.
(60) NIST X-Ray Photoelectron Spectroscopy (XPS) Database, Version 3.5. http://srdata.nist.gov/xps/ (accessed Jan 2011).
(61) Khairallah, F.; Glisenti, A. *Surf. Sci. Spectra* **2006**, *13*, 58.
(62) Aswal, D. K.; Muthe, K. P.; Tawde, S.; Chodhury, S.; Bagkar, N.; Singh, A.; Gupta, S. K.; Yakhmi, J. V. *J. Cryst. Growth* **2002**, *236*, 661.
(63) Chambers, S. A.; Tran, T. T. *Surf. Sci. Spectra* **1998**, *5*, 203.
(64) Goodrich, T. L.; Cai, Z.; Ziemer, K. S. *Appl. Surf. Sci.* **2008**, *254*, 3191.
(65) Benedetti, S.; Torelli, P.; Luches, P.; Gualtieri, E.; Rota, A.; Valeri, S. *Surf. Sci.* **2007**, *601*, 2636.
(66) Casey, P.; Hughes, G.; O'Connor, E.; Long, R. D.; Hurley, P. K. *J. Phys.: Conf. Ser.* **2008**, *100*, 042046.
(67) Brennan, B.; McDonnell, S.; Hughes, G. *J. Phys.: Conf. Ser.* **2008**, *100*, 042047.